Journal of Physics: Conference Series

PAPER • **OPEN ACCESS**

Calibration of strain gauges on a model runner blade combining numerical and experimental data

To cite this article: Johannes Kverno *et al* 2023 *J. Phys.: Conf. Ser.* **2629** 012009

Calibration of strain gauges on a model runner blade combining numerical and experimental data

Johannes Kverno[1]*, Igor Iliev[2], Bjørn Winther Solemslie[3] and Ole Gunnar Dahlhaug[1]

[1] Department of Energy and Process Engineering, Norwegian University of Science and Technology, Alfred Getz' vei 4, 7034 Trondheim, Norway
[2] SINTEF Energi AS, Sem Sælands vei 11, 7034 Trondheim, Norway
[3] NINA, Høgskoleringen 9, 7034 Trondheim, Norway

* E-mail: johannes.kverno@ntnu.no

Abstract. In this paper, we present the calibration setup, method, and results for a set of strain gauges installed on the trailing edge of the runner blades of a model Francis turbine. The calibration work is done as a step in the HydroFlex project, with the goal of taking experimental data to validate numerical models to better estimate the reduction in lifetime from more flexible operation. Due to the complex geometry of the blade, an analytical solution for the stresses for a given load is not possible to obtain, so calibration is needed. A combination of strain measurement and numerical analysis is used to correlate the response from the strain gauges directly to the strains parallel to the trailing edge. The strain gauges are installed on the suction side of the blades, and close to the hub and shroud, and the calibration is done by applying known weights on the shroud using a tailor made blade fixture. The signal from the sensors is passed through a set of miniature amplifiers that fits in the hub of the model runner. The numerical setup is done in ANSYS Mechanical, and is set up to fully replicate the conditions of the physical setup. The results shows that the method is viable, however there is a challenge with the response, and thus required amplification, due to the stiffness of the runner blade material.

1. Introduction

As the energy production transitions towards more renewable sources such as wind- and solar power, a higher demand for flexible operation is put on existing power plants, since solar- and wind power is non-dispatchable. Given the goal of reducing CO_2 emissions in the energy production sector, the remaining dispatchable power sources will need to vary their operation and power output even more to meet the demands on the grid. Hydro power is both highly dispatchable and a renewable energy source, meaning that it is well suited to fill the role of balancing the power grid as the output from wind- and solar power varies and the consumption goes up or down. In Norway, there are more than 1100 hydro power plants with an installed capacity of more than 1 MW [5]. The majority of these were designed for operation on a more or less constant power output and with a small number of load changes and start-stop cycles. The most common type of hydro turbine in use is the Francis turbine, and one major drawback of more off-design operation and start-stop cycles of these turbines is the increase in fatigue loading on the runner itself, meaning that a Francis turbine used for more flexible operation

schemes than it was designed for initially might need more maintenance and have unexpected and costly failures.
Due to the complex geometry of the runner blades, a simple analytical calculation of the strain at a certain location on the blade is not possible. In order to apply strain in the blade a force is applied at a small contact point by the use of weights, but to get a figure on the actual strain at the location of the strain gauges a numerical replication of the setup is used. The results of the finite element method (FEM) analysis is then used as the input in the regression analysis and a relationship between the strain in the blade and the strain gauge output is determined. In order to transmit the sensor output a slip ring is used, and therefor the signal is amplified before transmission, meaning that the output measured will be in volts.
This paper will focus on the calibration setup, procedure, and results of the strain gauges mounted on the trailing edge of a model Francis runner blade. A pair of pressure transducers have also been installed and calibrated, but since a static calibration of pressure is relatively standardised, an in depth description of the setup and method used will not be presented.

2. Calibration setup and instrumentation

The flexibility and operational constraints of any Francis turbine are largely dependent on the hydrodynamic and structural characteristics of the turbine's runner. For that reason, one of the tasks in the HydroFlex project is to combine structural and fluid-flow simulations in one design tool, which will support the process of designing more flexible Francis turbines for the future grid-balancing needs. This tool is fully automated to perform simulations on series of operating conditions [8], and employs optimization methods in parametric environment [3]. In order to asses the accuracy of the numerical results, and later improve the tool, an experimental model runner was designed and installed in the Waterpower laboratory at NTNU. Therefore, apart from the standard efficiency measurements which will be performed to validate the hydraulic optimization procedure, on-board measurements of the strain and dynamic loads on the runner blades will be performed over a wide operating range, during start/stop sequence, and rapid output adjustments.

2.1. Description of the model runner

According to the current state and possibilities in the laboratory, the measurement of the strain and dynamic loads on the runner blades is the most challenging task, and the experimental runner was primarily designed to fulfil several geometrical requirements that are expected to improve the measurements with strain gauges. These are:

- Fully supported blade from leading to trailing edge on both the hub and shroud sides. For validation purposes, this feature is expected to minimize uncertainties in the boundary conditions of the structural calculations.
- The runner blades must be as thin as possible to reduce the structural stiffness and provide larger blade deformation under the normal operating conditions of the turbine rig.
- The entire runner blade, especially the trailing edge, must have simple geometry that will make it easier for manufacturing with high accuracy and minimize the geometrical uncertainty. This resulted in low overall curvature of the blade, a trailing edge that is radial and without leaning, and a leading edge with only a small leaning.
- All blades must be detachable for easier instrumentation. Each blade section should have part of the hub and shroud as a single piece, which will be bolted together on common hub and shroud that are already available in the Waterpower laboratory.
- The runner must have a water-tight chamber inside the hub (center bushing) that will provide dry space for installation of on-board amplifiers and other electronics of the measuring chain.

The listed requirements pose significant geometrical restrictions in the design space of the runner, which will obviously affect and reduce the efficiency of the entire turbine. However, although the requirements for the hydraulic efficiency were relaxed and considered as secondary in the hydraulic optimization procedure, the tool was able to provide design which has efficiency on a comparable level with the original runner of the model turbine. The runner assembly is shown on Figure 1.

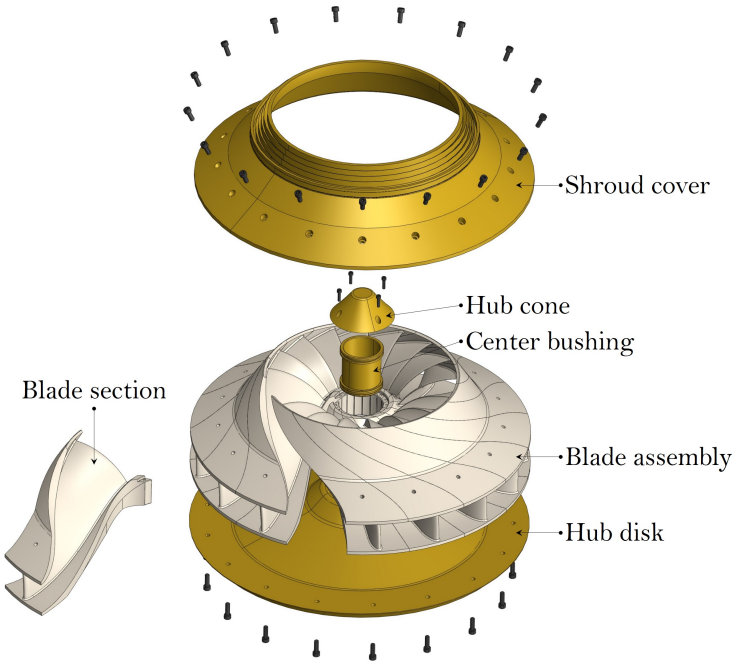

Figure 1. Exploded view of the runner assembly with isolated blade section. For simplicity, the on-board instrumentation is not shown.

2.2. Description of the custom blade fixture

Because the blade sections have complex and unique geometry, a custom blade fixture was designed to provide with the needed support, orientation and load location for the calibration procedure. The loading of the blade during operation is expected to cause higher static strain values on the gauge mounted close to the hub, and this was confirmed with initial high-fidelity CFD and FEA simulations. Due to this, the blade is bolted on the fixture using the bolt bores on the hub side of the section, and the loads were applied on the shroud side of the section. The orientation of the blade was adjusted so that the surface normal on the location where the loads are applied is directed vertically. The blade fixture is shown on Figure 2. The body of the blade fixture is over-dimensioned to provide with enough stiffness and stability during calibration, and was manufactured using 7075 Aluminium Alloy to reduce it's weight for easier handling in the laboratory. The pivot arm is made of S355 Non-Alloy Steel and is attached to the main body through a low friction SKF 607-2RSL closed ball bearing.

Both materials are selected to have slightly higher strength and slightly lower hardness than the material used for the blade section, which is JM7-15 Aluminium Bronze. The contact area between the arm and blade is dimensioned with enough margin to sustain twice the maximum required load before plastic deformation occurs on the arm. Under normal operating conditions

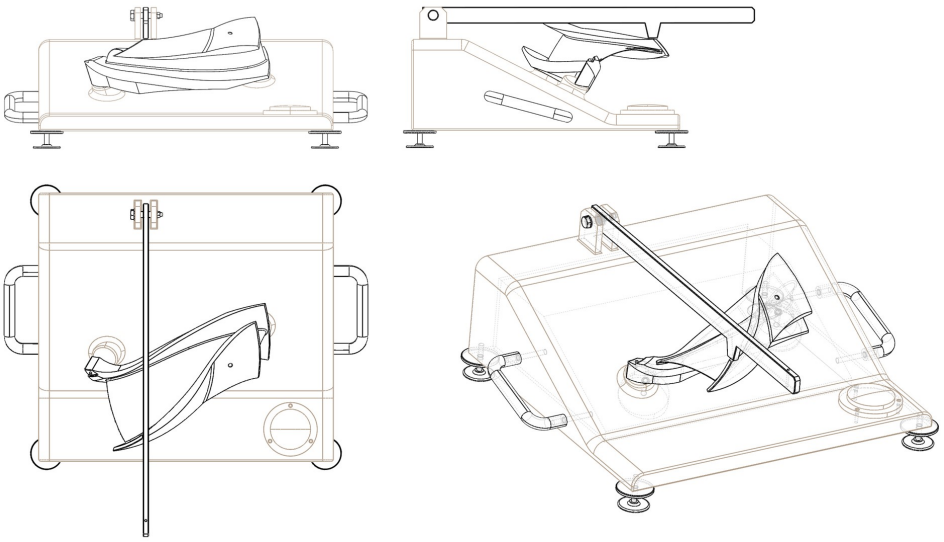

Figure 2. Orthographic and isometric views of the custom blade fixture designed for calibration of the strain gauges. The blade is bolted at two locations on the hub side and oriented to have a vertical direction of the surface normal at the location of the contact point with the arm. The fixture also has height adjustable legs and a spirit level gauge for horizontal adjustments before calibration.

of the model runner, the maximum principal elastic strains in the zone close to the trailing edges of the blades are nearly parallel to the trailing edge itself. This was confirmed by performing initial high-fidelity simulations within the HydroFlex project, and appears to be the case for other Francis turbines as well [1, 2, 9]. Therefore, the uni-directional strain gauges are also oriented parallel to the trailing edge, and outside of the characteristic trailing edge chamfer. During the design stage of the strain calibrator, the numerical results revealed that the applied loads will result in tensile strains for the hub gauge and compressive strain for the shroud gauge. On the contrary, the blade loading under normal operation will produce only tensile strains for both gauges mounted on the suction side of the blade. This reversed effect during the calibration procedure is due to the location of the contact point on the blade section, and can be mitigated to some extent by a trial-and-error re-positioning. On the other hand, the ductile material of the blade has nearly equal elastic modulus in both tensile and compression directions, and during normal operation of the turbine both gauges will be well inside the linear range of the sensors. Therefore, the strain reversal effect is considered to be negligible, and the calibration curves for both gauges can be used for tensile and compression strains.

2.3. Planned experiment and measurement chain

The goal for the planned experiment is to measure the strain at the trailing edge near both the hub and shroud on two of the runner blades, as well as pressure near the leading edge of one blade. With the sensors being installed in the rotating runner, it was chosen to also amplify the sensor outputs before transmitting them through a slip ring mounted on the shaft in order to reduce the noise to signal ratio. From the slip ring, the signal is fed into a couple of NI-cDAQ modules connected to a computer which also measures and records various inputs from the model test rig, as demonstrated in Figure 3. The recording is done in a custom LabVIEW program that also does some processing of the data on the fly. One alternative modification to the test setup which is under consideration is to reduce the amplification gain on the on-board

amplifiers to reduce the noise stemming from the amplifiers them selves, and then increase the amplification after the slip ring to utilise the full analog range of the DAQ input. This might keep the noise to signal ratio from the slip ring low enough, while avoiding introducing too much noise from the miniature amplifiers.

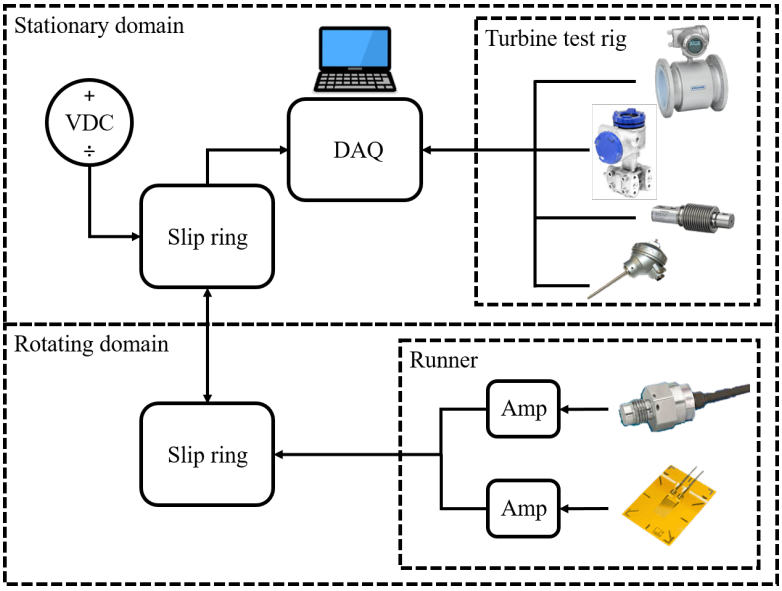

Figure 3. Illustration showing the measurement setup

2.4. Calibration setup and procedure

The calibration of the strain gauges is done by combining results from numerical simulations and measured results from the blade in the fixtureThe load is distributed with 10 points from minimum to maximum load starting with no weight applied, up to 15 kg hanging on the end of the arm of the fixture. It goes up in steps of 2 kg, except for near the end points. To check the repeatability of the measurements and any hysteresis, each point is taken four times, twice moving from a lower to a higher load, and twice moving from higher to lower. Due to the deformation of the arm itself it was found that a small horizontal force was applied to the blade as well as the intended vertical force, and the measurements would differ by an increasing amount as the applied weight increased, to the extent that the measured voltage differed by more than 10% at the highest load. One solution to this behaviour was to lubricate the contact surface between the shroud of the blade and the contact point of the fixture arm and allow the horizontal displacement of the arm. In addition to the lubrication, it was found that tapping the blade with the handle of a small screw driver was also required to make the arm settle and drastically reduce the horizontal forces, and doing this reduced the discrepancy of the measured voltage at the max weight point to less than 1% for the hub gauge.

3. Numerical analysis

To obtain the values of elastic strain for both strain gauge locations, the dead weight strain calibration procedure was simulated in ANSYS Mechanical. For different weights applied as boundary conditions, steady-state structural simulations were performed with the primary goal to calculate the uni-directional elastic strains, while secondary goals were to calculate and control-check the equivalent stresses and total deformation of the blade.

3.1. Numerical setup

To simplify the procedure, the blade and arm were simulated separately, where the structural response of the arm was simulated first, and then the results were used as boundary conditions for the simulation of the structural response of the blade. For the arm, remote displacement support was used at the hinge to allow rotation only about the pivot axis (where a ball bearing is installed), while the contact point with the blade had a friction-less support in the vertical z-axis. Vertical force was applied equivalent to the different weights that were applied on the physical setup. For the blade, fixed support was used on the internal walls of the bolt bores and vertical force was applied on the contact point with the arm. On Figure 4 shown is a graphical representation of the numerical setup, together with contours of exaggerated total deformation relative to a non-deformed state. Gravitational effects in the form of steady-state inertial forces were also included for the blade and arm, using the local gravitational constant. In this type of analysis, the loads do not induce significant inertia effects and damping, assuming slow variation in time of the loads and the structure's response and time invariant end results [4]. All details of the FEA configuration in ANSYS Mechanical are given in Table 1.

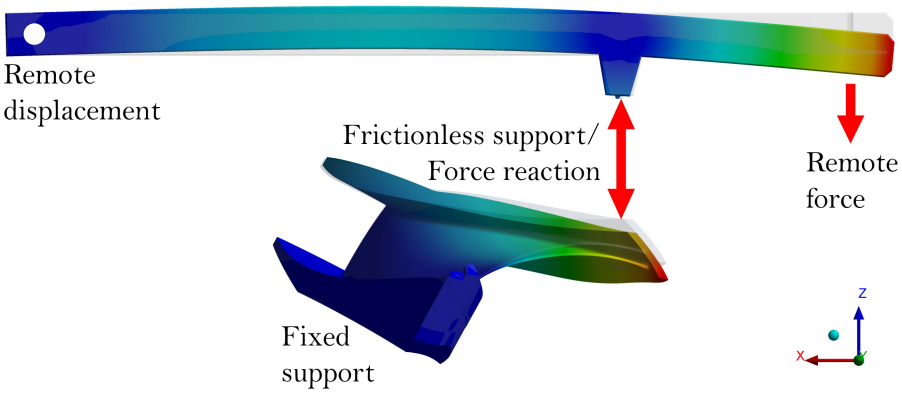

Figure 4. Boundary conditions for the structural setup. For demonstration purposes, the contours of the total deformation for the case with maximum weight applied is shown in scaled values, together with the non-deformed state. In true scale, the maximum deformation is less than 0.2 *mm* for the blade and the arm.

The strains that are detected by the physical uni-directional strain gauges are averaged [10] and, for the simulation of this effect, surface elements are used in the setup to average over the area of the gauge. In that sense, the gauge is numerically represented as a single shell element with bounded contact to the surface of the blade, which provides with the averaging effect needed. Element type SHELL181 was used due to it's suitability for analysing thin shell structures and membranes [4], with stiffness set to zero to eliminate it's effects on the stiffness of the blade itself. Therefore, the thickness of the element is irrelevant because the element has only four nodes, however, to create the element grid the thickness was arbitrarily set to 20 μm. Additionally, local coordinate systems were defined for each surface element, allowing to calculate the strain in the correct direction of the gauge that is to be used for the calibration procedure.

3.2. Estimation of uncertainty due to discretization

To estimate the discretization error in the structural simulations of the blade, the Grid Convergence Index (GCI) is used [6]. The GCI provides a uniform procedure for reporting results from grid refinement studies, and is based on an error estimator derived from the Richardson Extrapolation method [7].

Table 1. Configuration details in *ANSYS* Mechanical

	Blade	Strain gauge patch	Pivot arm
Analysis type	Static (steady-state)	Static (steady-state)	Static (steady-state)
Support	Fixed support	Bounded contact	Remote displacement, Friction-less support
Load	Normal force	Blade surface strain	Remote point force
Element size	0.63 mm	n/a	2 mm
Total elements	26512938	1	205159
Total nodes	36283766	4	301717
Element type	SOLID187	SHELL181	SOLID187
Grid type	Tetrahedral	Hexahedral	Tetrahedral
Solver type	Iterative	Iterative	Direct
Gravity	9.82146516 m/s^2	n/a	9.82146516 m/s^2
Temperature	20^oC	n/a	20^oC
Material	JM7-15 Aluminium Bronze	n/a	S355 Structural Steel
Young's modulus	118 GPa	n/a	210 GPa
Yield strength	300 MPa	n/a	335 MPa
Density	7600 kg/m^3	n/a	7850 kg/m^3
Mass	6.1423 kg	n/a	1.4757 kg

Due to the complexity of the geometry, tetrahedral grid with control of the global element sizing h was used to generate three computational grids of size N, with refinement factor $r = h_{coarse}/h_{fine}$ of approximately 1.35. A detail view of the grid density around both gauges, and for all three grid sizes, are shown on Figure 5. The refinement was done globally, i.e., systematically in all three directions, in such way that the finest grid would end-up using the entire memory resource of a workstation with 128GB of RAM available. The strain values ϕ for the hub and shroud gauges are the key variables, and the results for the maximum weight applied were used to estimate the errors. As can be seen from the summary given in Table 2, the fine grid has error of less than 0,5% for both gauges, and all calculations needed for the calibration were done with

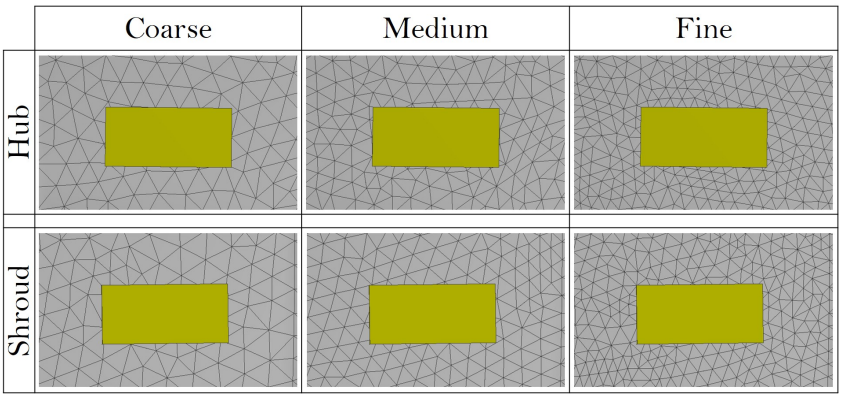

Figure 5. Detailed view of the computational grid close to the measuring zones of the strain gauges, and for the three grid resolutions used in the estimation of the discretization uncertainty. The strain calculated by the single element gauge (yellow) will be averaged upon the tetrahedral elements/nodes in contact.

this grid. The relations used to calculate all parameters in Table 2 are not repeated in this paper, and can be found in [6].

Table 2. Calculation of discretization error

Symbol	Hub strain gauge	Shroud strain gauge	Description	Unit
N_1	26.5M	26.5M	Grid size	-
N_2	10.78M	10.78M		-
N_3	4.39M	4.39M		-
r_{21}	1.3499	1.3499	Refinement factor	-
r_{32}	1.3493	1.3493		-
ϕ_1	109.9851	-16.6136	Microstrain	μm/m
ϕ_2	109.5226	-16.5656		μm/m
ϕ_3	108.5770	-16.4369		μm/m
p	2.3911	3.3014	Apparent order	-
ϕ_{ext}^{21}	110.4260	-16.6419	Microstrain	μm/m
e_a^{21}	0.42%	0.29%	Error	%
e_{ext}^{21}	0.40%	0.17%		%
GCI_{fine}^{21}	0.50%	0.21%	Grid convergence index	%

4. Calibration and uncertainty analysis

4.1. Calibration results

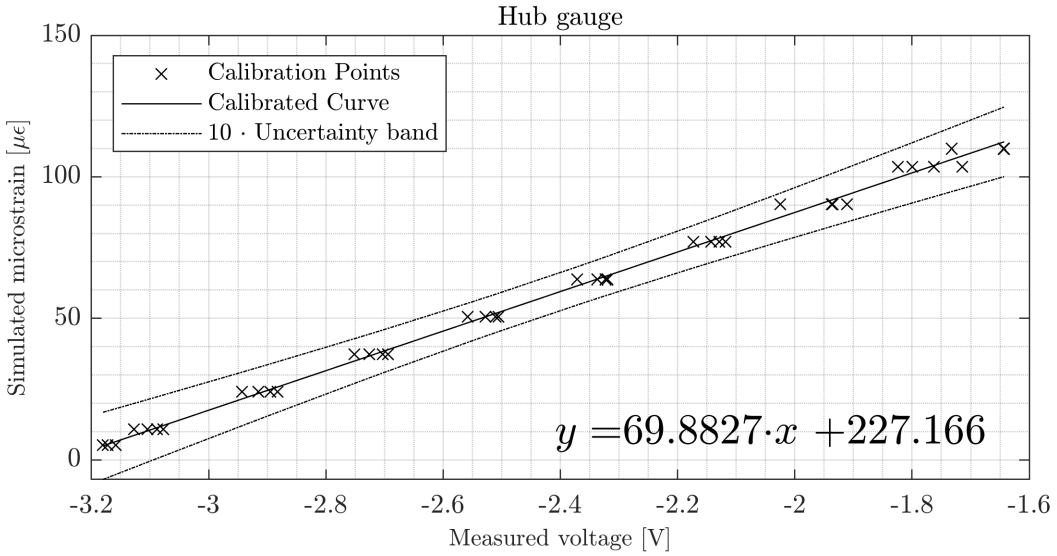

Figure 6. Calibration line, uncertainty bands and linear expression for the strain gauge near the hub side on the blade.

The results are also presented in Table 3 where X denotes the measured voltage, Y denotes the simulated strain, $f(X)$ denotes best fit, e_{tot} denotes the absolute total uncertainty, and f_{tot} denotes the relative total uncertainty. Subscript h refers to the strain gauge near the hub, and subscript s refers to the strain gauge near the shroud.

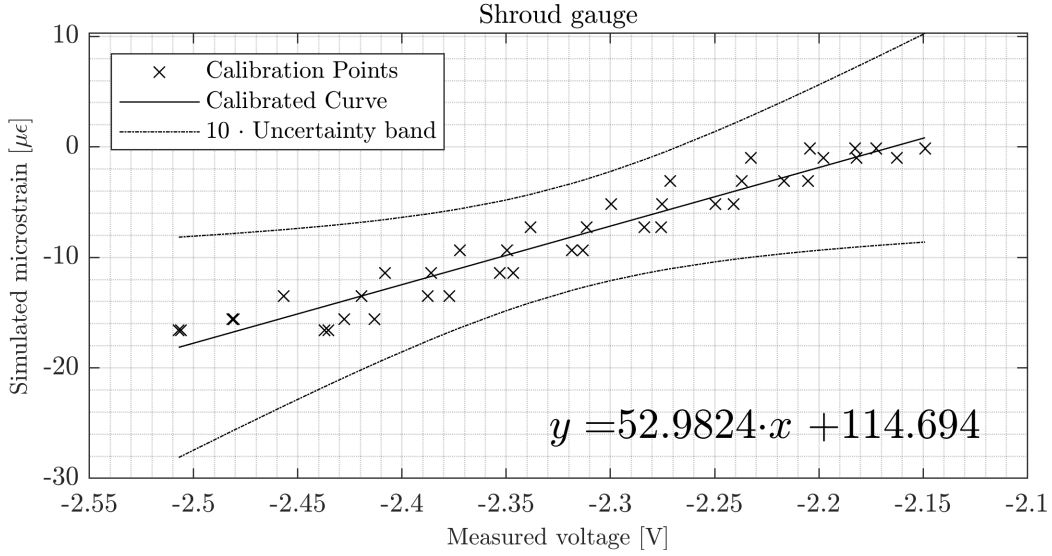

Figure 7. Calibration line, uncertainty bands and linear expression for the strain gauge near the shroud side on the blade.

4.2. Uncertainty analysis

To calculate the total uncertainty for each of the calibration points the root-sum-square of the random uncertainty and regression uncertainty was utilised. The random uncertainty was calculated by

$$e_{rand} = \frac{t_{\alpha/2} \cdot s}{\sqrt{N}} \tag{1}$$

where $t_{\alpha/2}$ is the t value with a confidence level set to $97,5\%$, s is the standard deviation of the sampled data for one point, and N is the total number of samples for said measurement. The regression uncertainty is calculated after finding the linear fit for the measured points by calculating the variation in both x and y direction individually, and both direction combined.

Table 3. Calibration data from the both strain gauges.

X_h [V]	Y_h [μm/m]	$f(X_h)$ [μm/m]	$e_{h,tot}$ [μm/m]	$f_{h,tot}$ [%]	X_s [V]	Y_s [μm/m]	$f(X_s)$ [μm/m]	$e_{s,tot}$ [μm/m]	$f_{s,tot}$ [%]
-3,172	5,164	5,475	1,178	22,81	-2,204	-0,120	-2,098	-0,733	610,66
-3,127	10,765	8,617	1,130	10,50	-2,232	-1,001	-3,593	-0,639	63,86
-2,943	24,016	21,474	0,947	3,94	-2,271	-3,086	-5,647	-0,538	17,43
-2,751	37,268	34,912	0,789	2,12	-2,299	-5,171	-7,145	-0,494	9,56
-2,558	50,520	48,393	0,690	1,37	-2,338	-7,256	-9,202	-0,489	6,75
-2,370	63,766	61,479	0,675	1,06	-2,372	-9,341	-10,986	-0,538	5,76
-2,173	77,016	75,279	0,750	0,97	-2,408	-11,425	-12,902	-0,632	5,53
-2,025	90,266	85,638	0,855	0,95	-2,456	-13,510	-15,475	-0,798	5,91
-1,799	103,520	101,406	1,064	1,03	-2,480	-15,596	-16,740	-0,890	5,71
-1,732	109,985	106,106	1,134	1,03	-2,506	-16,613	-18,087	-0,992	5,98
-1,732	109,985	106,093	1,134	1,03	-2,507	-16,613	-18,141	-0,997	6,00
-1,824	103,520	99,700	1,040	1,00	-2,481	-15,596	-16,779	-0,893	5,73
-1,937	90,266	91,780	0,931	1,03	-2,419	-13,510	-13,499	-0,667	4,94
-2,142	77,016	77,409	0,769	1,00	-2,385	-11,425	-11,720	-0,570	4,99
-2,337	63,766	63,848	0,681	1,07	-2,349	-9,341	-9,790	-0,500	5,36
-2,528	50,520	50,498	0,682	1,35	-2,311	-7,256	-7,773	-0,485	6,69
-2,725	37,268	36,686	0,772	2,07	-2,275	-5,171	-5,849	-0,530	10,26
-2,915	24,016	23,447	0,921	3,84	-2,237	-3,086	-3,828	-0,626	20,28
-3,104	10,765	10,207	1,106	10,28	-2,197	-1,001	-1,749	-0,756	75,57
-3,180	5,164	4,913	1,186	22,98	-2,182	-0,120	-0,949	-0,812	676,79
-3,172	5,164	5,492	1,177	22,81	-2,172	-0,120	-0,403	-0,852	709,64
-3,088	10,765	11,349	1,089	10,12	-2,181	-1,001	-0,907	-0,815	81,45
-2,894	24,016	24,892	0,903	3,76	-2,216	-3,086	-2,755	-0,690	22,37
-2,703	37,268	38,265	0,758	2,04	-2,249	-5,171	-4,495	-0,590	11,41
-2,510	50,520	51,704	0,678	1,34	-2,283	-7,256	-6,308	-0,515	7,10
-2,323	63,766	64,818	0,685	1,07	-2,318	-9,341	-8,142	-0,483	5,18
-2,129	77,016	78,372	0,778	1,01	-2,353	-11,425	-9,981	-0,505	4,42
-1,935	90,266	91,914	0,933	1,03	-2,387	-13,510	-11,807	-0,574	4,25
-1,762	103,520	103,966	1,102	1,06	-2,427	-15,596	-13,935	-0,694	4,45
-1,644	109,985	112,259	1,229	1,12	-2,435	-16,613	-14,338	-0,720	4,34
-1,642	109,985	112,357	1,230	1,12	-2,437	-16,613	-14,429	-0,726	4,37
-1,714	103,520	107,336	1,152	1,11	-2,413	-15,596	-13,164	-0,647	4,15
-1,911	90,266	93,596	0,955	1,06	-2,377	-13,510	-11,256	-0,549	4,07
-2,117	77,016	79,162	0,786	1,02	-2,346	-11,425	-9,641	-0,497	4,35
-2,319	63,766	65,073	0,686	1,08	-2,313	-9,341	-7,867	-0,485	5,19
-2,505	50,520	52,067	0,677	1,34	-2,275	-7,256	-5,873	-0,529	7,30
-2,694	37,268	38,872	0,753	2,02	-2,240	-5,171	-4,028	-0,614	11,89
-2,882	24,016	25,741	0,892	3,72	-2,205	-3,086	-2,141	-0,730	23,66
-3,077	10,765	12,124	1,078	10,01	-2,162	-1,001	0,116	-0,890	88,92
-3,158	5,164	6,420	1,163	22,53	-2,149	-0,120	0,831	-0,944	786,50

5. Conclusion

In the future, hydro turbines will be operated at off load condition, and this will reduce their lifetime due to fatigue loads. Therefore, it is crucial for an owner of turbines to know their remaining lifetime at all times. The remaining lifetime can be calculated from fatigue loads on the turbine, and this is the reason why this paper is focusing on the measurements of stress and strain in hydro turbine runners. In order to measure the of hydro turbines The calibration method in this paper represent a new method for calibration of strain gauges in Francis model turbines. The method of using numerical analysis of the strain for calibration has never been used by personnel at the Waterpower Laboratory at NTNU earlier. It is the lack of other alternatives that gave this method a chance. However, with high quality numerical results, it has proven to be a good alternative for future calibrations.

6. Acknowledgements

The work has been performed as part of the HydroFlex project, and received funding from the European Union's Horizon 2020 research and innovation programme under grant agreement No 764011. The authors would like to thank EDR&Medeso AS for providing numerical results of harmonic response analysis for the runner, which were used for positioning and selection of the strain gauges.

References

[1] Halvard Bjørndal, Trond Moltubakk, and Hans Aunemo. "Flow induced stresses in a medium head Francis runner – Strain gauge measurements in an operating plant and comparison with Finite Element Analysis". In: June 2001.

[2] Eduard Doujak and Markus Eichhorn. "An Approach to Evaluate the Lifetime of a High Head Francis Runner". In: 2016.

[3] Igor Iliev et al. "Optimization of Francis Turbines for Variable Speed Operation Using Surrogate Modeling Approach". In: *Journal of Fluids Engineering* 142.10 (Aug. 2020). 101214. ISSN: 0098-2202. DOI: 10.1115/1.4047675. eprint: https://asmedigitalcollection.asme.org/fluidsengineering/article-pdf/142/10/101214/6554501/fe_142_10_101214.pdf. URL: https://doi.org/10.1115/1.4047675.

[4] ANSYS Inc. *ANSYS Mechanical APDL product documentation*. Release 18.2. 2017.

[5] NVE. *Vannkraft*. 2022. URL: https://www.nve.no/energi/energisystem/vannkraft/ (visited on 03/08/2022).

[6] "Procedure for Estimation and Reporting of Uncertainty Due to Discretization in CFD Applications". In: *Journal of Fluids Engineering* 130.7 (July 2008). 078001. ISSN: 0098-2202. DOI: 10.1115/1.2960953. eprint: https://asmedigitalcollection.asme.org/fluidsengineering/article-pdf/130/7/078001/5491455/078001_1.pdf. URL: https://doi.org/10.1115/1.2960953.

[7] P. J. Roache. "Perspective: A Method for Uniform Reporting of Grid Refinement Studies". In: *Journal of Fluids Engineering* 116.3 (Sept. 1994), pp. 405–413. ISSN: 0098-2202. DOI: 10.1115/1.2910291. eprint: https://asmedigitalcollection.asme.org/fluidsengineering/article-pdf/116/3/405/5531128/405_1.pdf. URL: https://doi.org/10.1115/1.2910291.

[8] Erik Tengs et al. "Fully automated multidisciplinary design optimization of a variable speed turbine". In: *IOP Conference Series: Earth and Environmental Science* 774.1 (June 2021), p. 012031. DOI: 10.1088/1755-1315/774/1/012031. URL: https://doi.org/10.1088/1755-1315/774/1/012031.

[9] Julian Unterluggauer, Eduard Doujak, and Christian Bauer. "Fatigue analysis of a prototype Francis turbine based on strain gauge measurements". In: *WASSERWIRTSCHAFT* 109 (Sept. 2019), pp. 66–71. DOI: 10.1007/s35147-019-0238-9.

[10] N. Younis and B. Kang. "Averaging effects of a strain gage". In: *Journal of Mechanical Science and Technology* 25 (Mar. 2011), pp. 163–169. DOI: 10.1007/s12206-010-1020-1.